Sensors and Materials, Vol. 25, No. 5 (2013) 309–321
MYU Tokyo

S & M 0922

Electrical Conductivity and Hysteresis Characteristic of $BaTiO_3$-Based Sensors with Polymethyl metacrylate (PMMA) Pore Former

Burcu Ertuğ*

Department of Metallurgical and Materials Engineering, Istanbul Technical University, 34469 Maslak, Istanbul, Turkey

Key words: Barium titanate, sintering, microstructure, PMMA, electrical conductivity, hysteresis

(Received May 29, 2012; accepted October 9, 2012)

Porous barium titanate ceramics were fabricated by the addition of polymethyl metacrylate (PMMA). The effects of PMMA on the microstructure and electrical conductivity of the porous ceramics were investigated. According to thermal analysis, the endothermic reaction occurred at 832.7°C, which corresponds to the orthorhombic-hexagonal transformation of barium carbonate, and the formation of barium titanate occurred at 1098.6°C. It was found that the porosity increased and the grain size decreased with increasing PMMA mass%. The crystalline structure of barium titanate ceramics was determined to be tetragonal and independent of PMMA content. The electrical conductivity, humidity sensitivity, and hysteresis characteristic of fabricated ceramics changed with relative humidity, porosity, and PMMA content.

1. Introduction

The control and adjustment of humidity are important for daily life and a number of industrial processes. One of the most unwanted humidity sensor characteristics is hysteresis. Hysteresis for a given humidity sensor can be defined as the difference in sensor output between increasing and decreasing humidity percentage.[1,2] Hysteresis includes two different transfer functions of the same humidity-sensing element. Humidity sensors with small hysteresis are useful for precise readings. Hysteresis determines the repeatability of a humidity sensor. The hysteresis depends on the total span of the humidity cycle, exposure time, temperature and sensor production. Usually, sensor hysteresis increases as the sensor is exposed to high humidity and high temperature over

*Corresponding author: e-mail: burcuertug@gmail.com

long periods of time. Another sensor characteristic related to hysteresis is the accuracy limits of the sensor. When the accuracy of an instrument is specified, half the maximum hysteresis should be equally distributed as positive and negative errors. The accuracy limits of a humidity sensor show the deviations from the ideal transfer function of the sensing element.[3–5]

2. Materials and Methods

High-purity $BaCO_3$, TiO_2 and La_2O_3 (>99%, Merck KGaA, Germany) ceramic powders were utilized in this study. The barium titanate ceramics obtained contain 0.3 mol% La_2O_3. The polymethyl metacrylate (PMMA) (powder form, Mw = 120,000 gr., Sigma-Aldrich) was used as the pore former.

Table 1 shows the compositions of the samples before the sintering. Except BT, the nominal composition of the other samples was $Ba_{1-x}La_xTiO_3$ after sintering. The powders were then mixed in a plastic jar for 24 h. The mixed powders were compacted by unaxial cold pressing at a pressure of 40 MPa to prepare the green compacts (15 × 12 × 7 mm^3). The sintering parameters and grain size and porosity were given in Table 2. The sintering was carried out by heating and cooling at rates of 5 and 10°C/min, respectively, in air using a Protherm high-temperature furnace. Differential thermal analysis (DTA) and thermogravimetric analysis (TGA) of the ceramics were performed in air, using a thermal analyzer (DTA/TGA Netzsch 409 PC) at a heating rate of 10°C/min. The microstructure and crystalline structure of the barium titanate ceramics were analyzed by scanning electron microscopy (SEM) and X-ray diffraction (XRD), respectively. An X-ray diffractometer (Bruker D8 Advance system with Cu-K_α radiation (λ = 1.54 Å)) was used to characterize the phase composition of the specimens. XRD analysis was carried out on as-sintered and polished samples. The average grain size of the ceramics was estimated by the linear intersection method. The porosities were determined by Archimedes' method. The specimens were polished, cleaned using an ultrasonic bath and electroded using ohmic silver electrodes. The electrical resistances were measured using a standard multimeter (Digital Multimeter DY-64) by a 2-probe measurement method in a humid environment (Heraeus/Vötsch-HC 4033). For each of the three compositions, two transfer functions of the humidity-sensing element were measured

Table 1
Compositions of the samples used in this study before sintering.

Sample code	Composition before sintering (wt%)			
	$BaCO_3$	TiO_2	La_2O_3	PMMA
BT	71.09	28.90	—	—
BTL	70.97	28.86	0.18	—
BTLP-1	70.37	28.62	0.18	1.00
BTLP-2	69.94	28.44	0.17	1.75
BTLP-3	69.50	28.26	0.17	2.50

Table 2
Grain size and porosity of sintered samples.

Sample code	Grain size (μm)	Porosity (%)	T_{sinter} (°C)	t_{sinter} (h)
BTLP-1	6.3	33.2	1300	2
BTLP-2	6	35.2	1300	2
BTLP-3	5.8	37.3	1300	2
BTLP-1	7.57	29.6	1300	6
BTLP-2	7.29	31.4	1300	6
BTLP-3	7	33.4	1300	6
BTLP-1	12.3	16.9	1500	2
BTLP-2	11.8	18.7	1500	2
BTLP-3	11.4	19.95	1500	2
BTLP-1	14.87	15.2	1500	6
BTLP-2	14.3	16.55	1500	6
BTLP-3	13.75	17.9	1500	6

with ascending and descending humidity percentages. Humidity sensitivity cycles were given with humidity percentage. The accuracy limits of the humidity sensor were shown on the cycle curve. All the hysteresis cycles were carried out at room temperature except for the composition with 2.5 wt%, the cycle curve was also given at 60 and 80°C.

3. Results

The microstructures of the as-sintered samples are shown in Fig. 1. After doping 0.3 mol% La_2O_3, the grain size decreased markedly. The grain size of the pure barium titanate sample was 16.5 μm, as shown in Fig. 1(a), whereas that of the La_2O_3-doped barium titanate sample was 5.5 μm. Table 2 briefly gives the grain size and porosity of sintered samples.

The thermal analysis curve of BTLP-3 is given in Fig. 2. DTA results were obtained up to 1200°C, which is the lowest sintering temperature for the compositions studied. For BTLP-3, the endothermic reaction occurred at 832.7°C, which corresponds to the orthorhombic-hexagonal transformation of barium carbonate.[6] The formation of barium titanate occurred at 1098.6°C for BTLP-3. Two other reactions were present in the DTA curve of BTLP-3, which contains 2.5 wt% PMMA. The first endothermic reaction represents the phase transition of PMMA and the other exothermic reaction shows the decomposition of random chains of PMMA at 357.6°C.

Figure 3 shows the XRD diagram of the samples sintered at 1200°C. As the sintering duration increased from 2 to 6 h at 1200°C, the intensity of the XRD diagram increased. This was valid for all the sintering temperatures studied. (101) plane reflection is observed in Fig. 3, which has the maximum intensity at 2θ = 36.701°, and the plane distance is determined to be 2.8412 Å. In Figs. 2 and 3, a split peak is observed at 2θ = 52.595 and 53.220°, corresponding to (002) and (200) plane reflections, which is not observed in the cubic symmetry of barium titanate and is used for the determination of

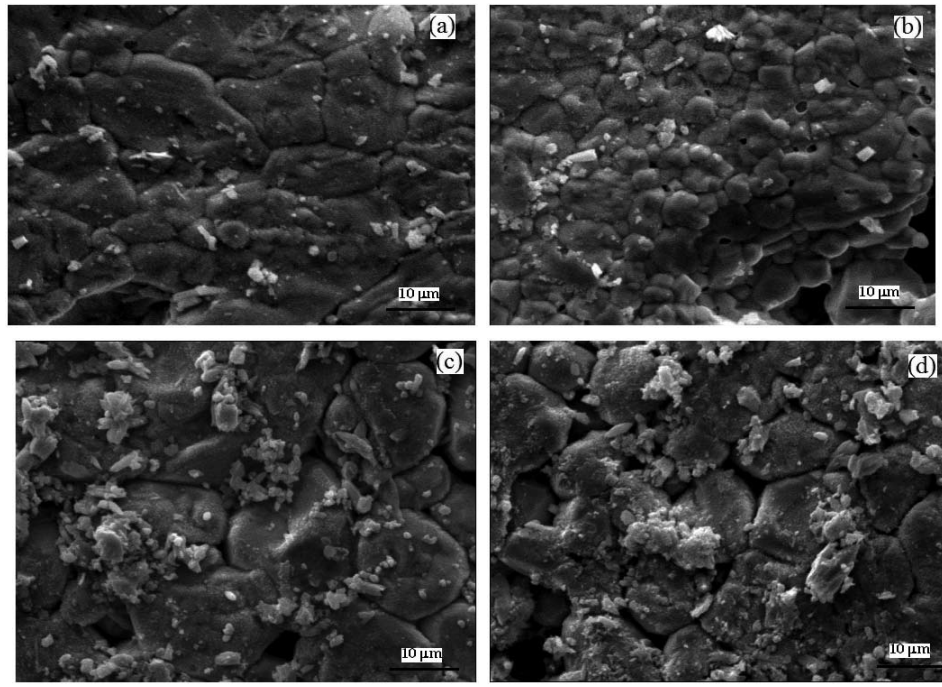

Fig. 1. SEM images for (a) pure, (b) La_2O_3-doped barium titanate, (c) BTLP-1, and (d) BTLP-3, 1500°C for 6 h (×2000).

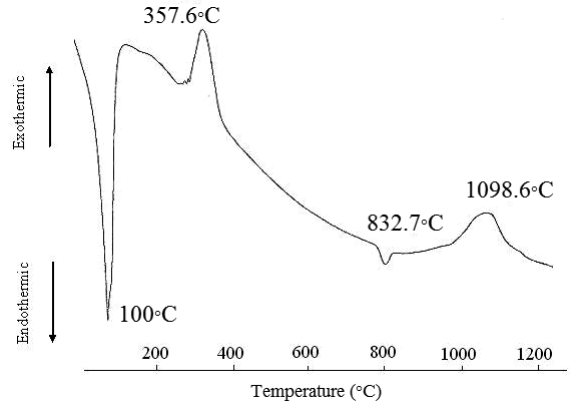

Fig. 2. Differential thermal analysis curve for BTLP-3.

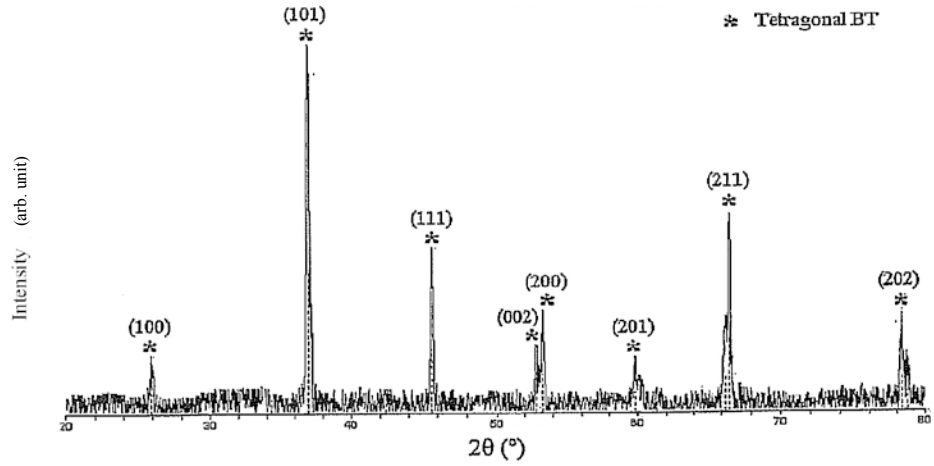

Fig. 3. XRD diagram of BTLP-3 sintered at 1300°C for 4 h.

tetragonal and cubic crystal structures. The plane distances of (002) and (200) reflections are determined using Joint Committee for Powder Diffraction Standards (JCPDS) card number 05-0626 as 2.0190 and 1.9970 Å, respectively.

The grain sizes of the fabricated barium titanate samples are given in Fig. 4. PMMA addition resulted in a slight grain refinement. The porosities of the samples are given in Fig. 5. As the PMMA content increased, the porosity increased linearly.

In Fig. 6(a), the transfer function of the sensing element is an exponential curve. BTLP-1 and BTLP-3 were sintered at 1200°C for 2 h and the transfer function of BTLP-2 was omitted for clarity. Both BTLP-1 and BTLP-3 indicated a saturation limit on their transfer functions. The electrical conductivity vs relative humidity for both compositions was high.

Upon sintering at 1300°C for 2–6 h, the maximum electrical conductivity was determined to be $10^{-3.8}$ S/m and was measured for BTLP-3 sintered for 2 h. The maximum conductivity obtained for the compositions sintered at 1500°C was measured to be $10^{-5.25}$ S/m and determined for BTLP-3 sintered for 2 h. The dead band regions were detected up to relative humidities of 40 and 60% for BTLP-1 sintered for 2 and 6 h, respectively. BTLP-3 sintered at 1500°C for 6 h also showed a dead band region up to a relative humidity of 40%, whereas that sintered for 2 h did not show a dead band region but its electrical conductivity was low and its linearity characteristic was poor.

Humidity sensitivity vs relative humidity graphs are also given in Fig. 7. Each value in the curves represents a ratio of the electrical resistance measured in air to that measured in a humid environment. In Fig. 7(a), there is a marked increase in humidity sensitivity up to a relative humidity of 80%. After this value, the increase in humidity sensitivity is limited and this is valid for both BTLP-1 and BTLP-3 sintered at 1200°C for

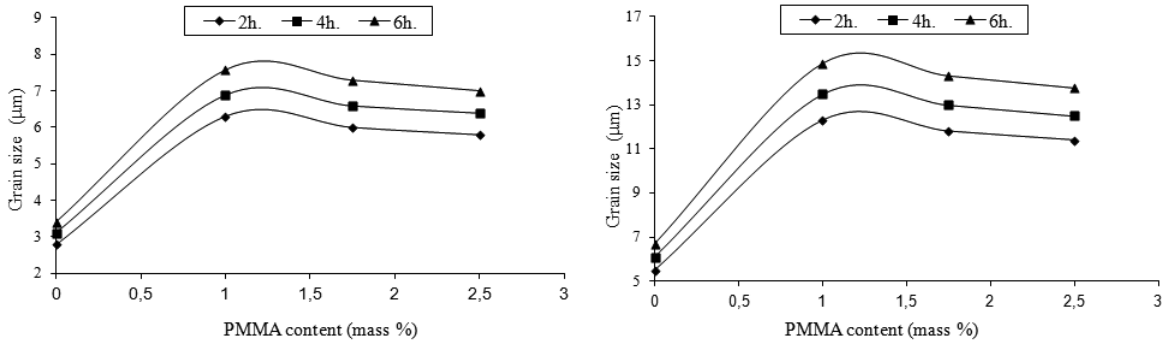

Fig. 4. Grain size vs PMMA content for (a) 1300 and (b) 1500°C.

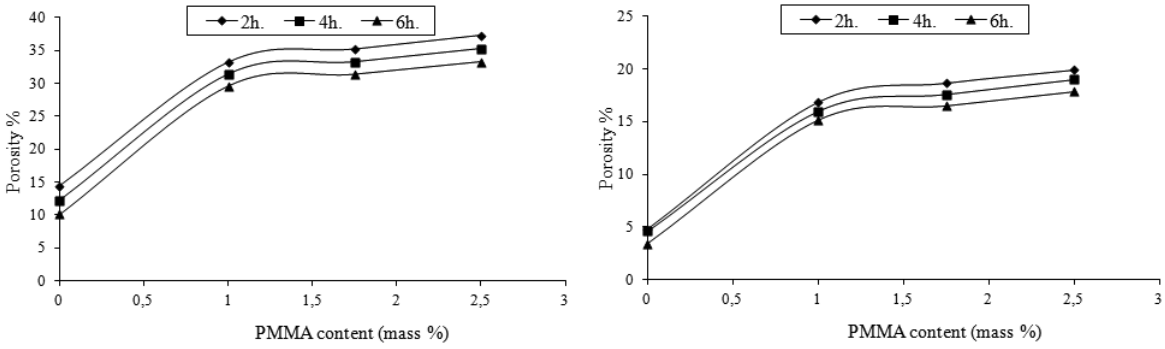

Fig. 5. Porosity vs PMMA content for (a) 1300 and (b) 1500°C.

2–6 h. For the samples sintered at 1300°C for 2–6 h, the maximum humidity sensitivity was determined to be 1.9, which means that the sensitivity increased approximately on the order of 100 when the sample was exposed to a relative humidity of 98%. For the samples sintered at 1400 and 1500°C, humidity sensitivity curves showed a negative exponential tendency, except that the samples sintered at 1500°C indicated a dead band region where the humidity sensitivity is equal to 1.

The linearity was high for BTLP compositions, which describes the working range of the sensing element. Figure 8 indicates the hysteresis curve for BTLP-3. In the hysteresis graph, the continous line shows the adsorption process (from low humidity to high humidity). For the compositions studied, the maximum humidity hysteresis was a relative humidity of 5%. For PMMA compositions, the electrical conductivities

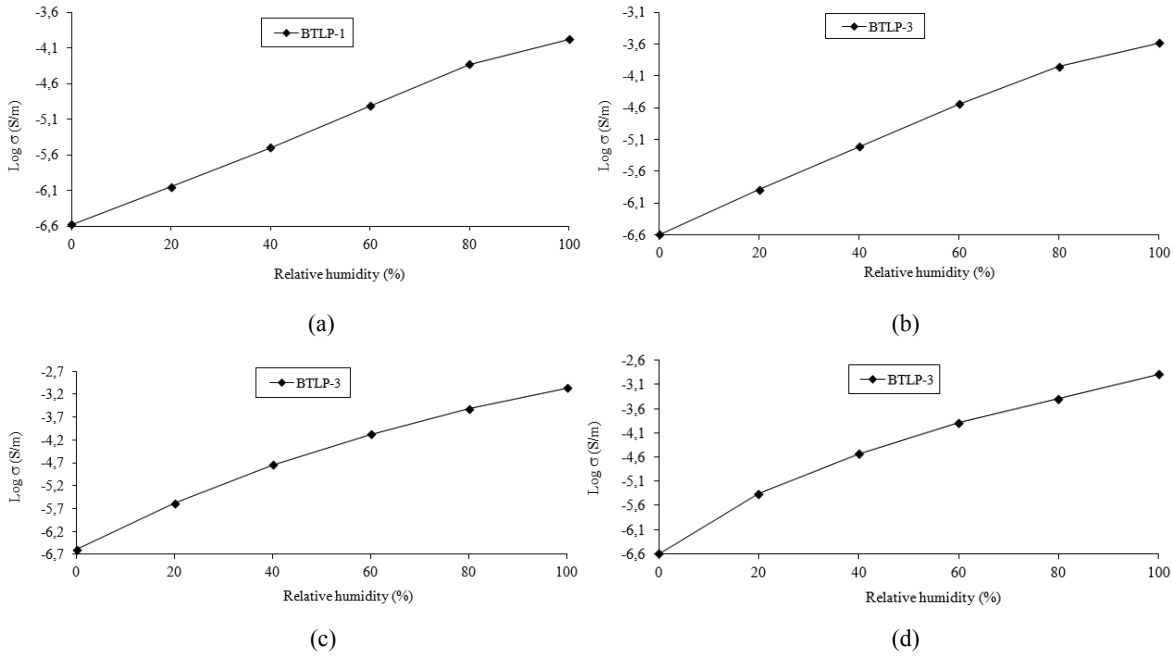

Fig. 6. Electrical conductivity vs relative humidity curves of BTLP compositions after 1300ºC for 2 h at (a) and (b) 20, (c) 60, and (d) 80°C.

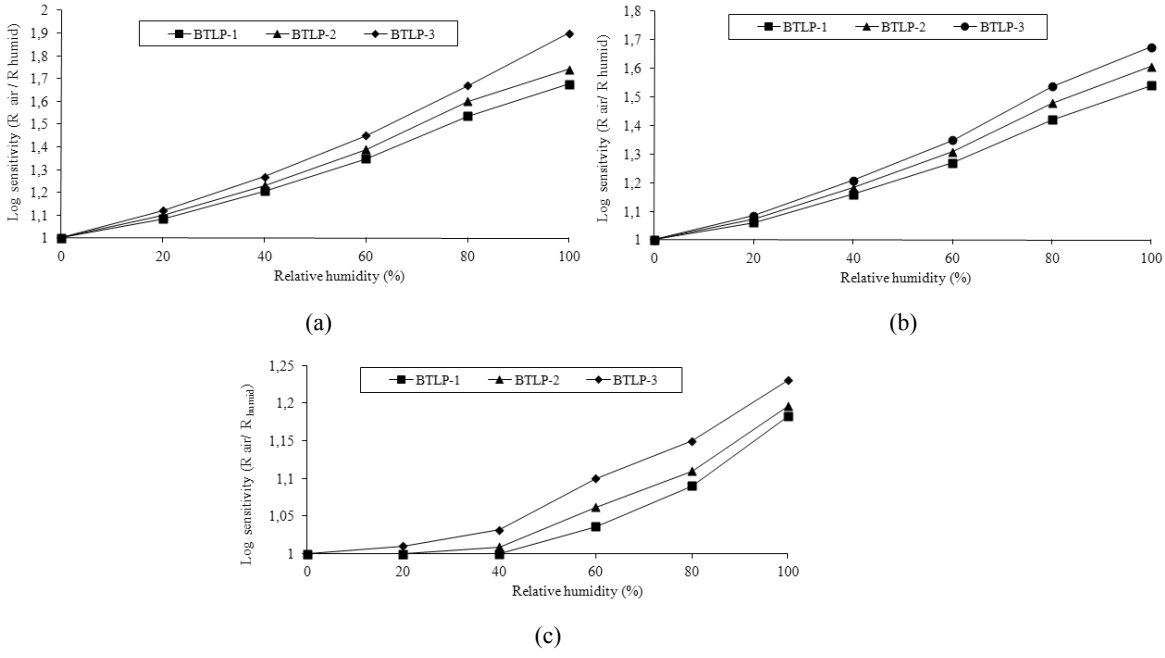

Fig. 7. Humidity sensitivity vs relative humidity curves of BTLP compositions after (a) 1300°C for 2 h, (b) 1300°C for 6 h, and (c) 1500°C for 2 h.

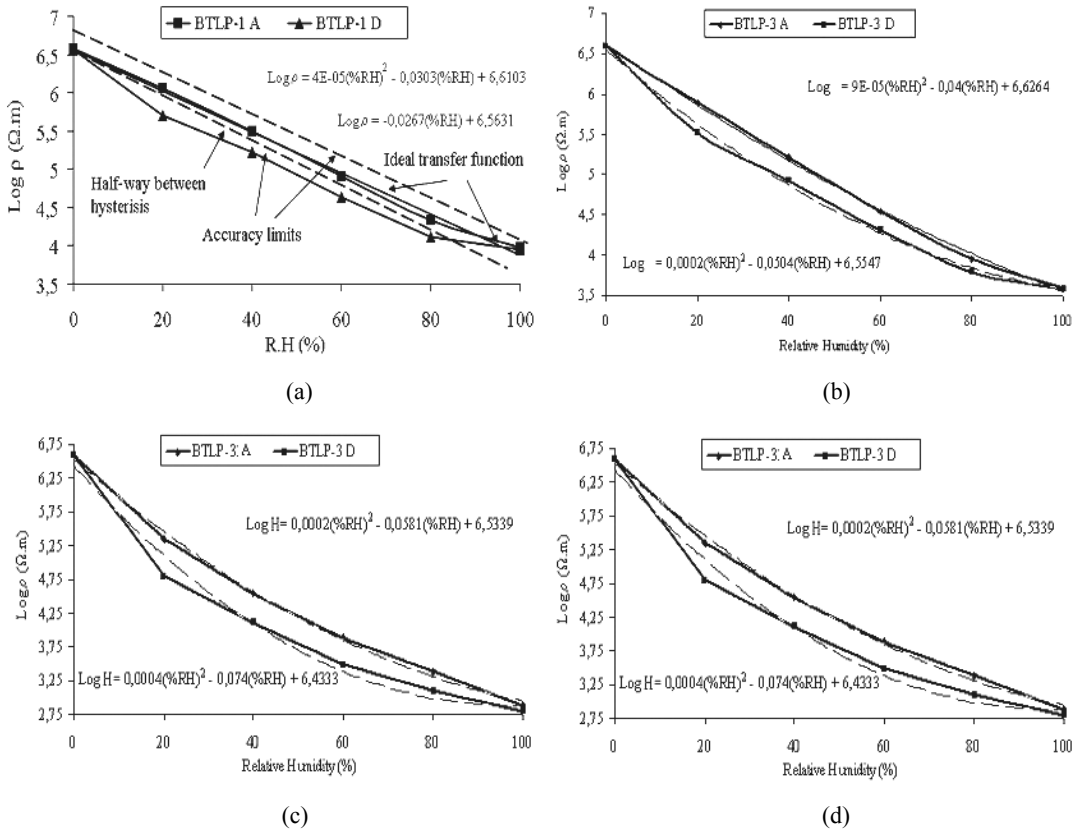

Fig. 8. Hysteresis curves of BTLP compositions after 1300°C for 2 h at (a)–(b) 20, (c) 60, and (d) 80°C.

increased with porosity. In the transfer functions, with increasing porosity, the saturation limit was reached. After the saturation limit was reached, the electrical conductivity did not change markedly and linearity degraded. The highest linearity was observed for BTLP, which was sintered at 1300°C. The linear region of the transfer function shows the practical application range of the sensing element.

As shown in Fig. 8, the transfer function of adsorption and desorption processes is $\text{Log } R = \alpha(\%\text{RH})^2 + \beta(\%\text{RH}) + \gamma$. The linear approximation of the transfer function of the adsorbtion process for BTLP-3 (sintered at 1300°C for 2 h) is $\text{Log } R = \alpha(\%\text{RH}) + \beta$.

Response and recovery times of BTLP-3, which contains 2.5 wt% PMMA, sintered at 1300°C for 2 h are given in Fig. 9. The time required to reach a stable electrical resistance can be determined using the data in Fig. 9.

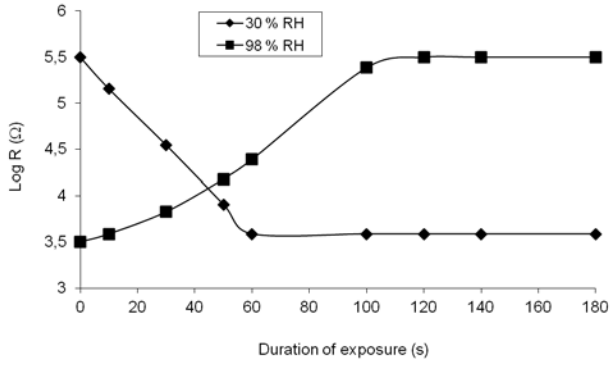

Fig. 9. The electrical resistance vs duration of exposure to humidity.

4. Discussion

There is a pronounced grain growth upon high-temperature sintering after 1500°C for 6 h. Doping 0.3 mol% La_2O_3 resulted in microstructural refinement. The grain size decreased, as shown in Fig. 1(b). 0.3 mol% is the threshold concentration of La_2O_3 doping, after which the grain size decreases and the electrical resistance increases. Peng and Lu studied the grain size and electrical conductivity vs La_2O_3 dopant concentration. They found that when barium titanate is doped with 0.3 mol% La_2O_3, it is transformed from semiconductor to insulator.[7] In the study of Qi *et al.*, donor-doped barium titanate exhibited semiconductor behaviour when sintered at and above 1300°C.[8] According to Brzozowski and Castro, a high donor content (above 0.15 mol%) resulted in a high resistivity.[9] Chatterjee *et al.* found that after 0.2 mol% donor doping, the electrical resistivity reached $10^{-6} – 10^{-7}$ S/m.[10]

The PMMA-containing samples included 0.3 mol% La_2O_3. Thus, they had a high electrical resistance in air atmosphere and a high surface area because of doping. PMMA addition also resulted in a slight grain refinement. Also, at lower sintering temperatures, PMMA addition caused a grain size inhibition. The pore elimination was valid for all the sintering durations at 1500°C. This could be explained by the rapid increase in the grain growth kinetics of the samples when sintered up to 1500°C. At lower sintering temperatures (except 1500°C), SEM images showed uniformly distributed pores in the matrix. Spaces were observed between the pores, and intergranular pore morphology was present. However, after sintering at 1500°C, the porosity was eliminated and the grain size increased significantly. The porosity of BTLP-1 was 15.2% when sintered at 1500°C for 6 h and that of BTLP-3 was 17.9%. SEM images in Figs. 1(c) and (d) were taken from the regions with the lowest porosity.

The plane distances of (002) and (200) reflections were determined using JCPDS card number 05-0626 as 2.0190 and 1.9970 Å, respectively. Since all the compositions studied consist of a constant amount of La_2O_3, split peaks of tetragonal barium titanate

gradually merged upon doping. This could be explained by the modification of the crystal symmetry of the tetragonal phase. Following the doping of fabricated barium titanate ceramics, a pseudocubic crystal symmetry was formed. The reason for the merging of peaks could be the internal stresses formed via the doping process. However, the amount of doping was not sufficient to transform the room-temperature tetragonal barium titanate phase to a cubic symmetry.

As shown in Fig. 10, (004) and (400) reflections of the high-angle XRD indicated that the split peaks merge upon donor doping. It was clear that all the as-sintered ceramics studied, whether pore-forming agent (PFA)-containing (PMMA) or only donor dopant, showed a tetragonal perovskite structure, irrespective of the added PFA content. As a result, the room-temperature crystal structure of porous $BaTiO_3$ ceramics was determined to be independent of the addition, doping or amount of the pore-forming agent. On the other hand, PFA-added compositions did not contain residual carbon (invisible as XRD reflections) besides the barium titanate phase. XRD peaks of BTLP-3 did not show considerable shifting as compared with those of BTLP-1. There was no evolution of a secondary phase owing to the existence of PFA addition. It was concluded that all the compositions studied contained variable percentages of porosity with a single perovskite $BaTiO_3$ phase.

The transfer function curves for PMMA-containing barium titanate ceramics are given in Fig. 6. Since the linearity, dead band region and saturation limit characteristics are the main parameters affecting the practical sensor applications, the sintering temperature was determined to be the main parameter for changing the availability of different compositions for several uses. The linearity characteristics of BTLP samples were high (indicated by R^2). However, there is a slight saturation limit for all the compositions studied. The saturation started after a relative humidity of 80%, as shown in Fig. 6. The

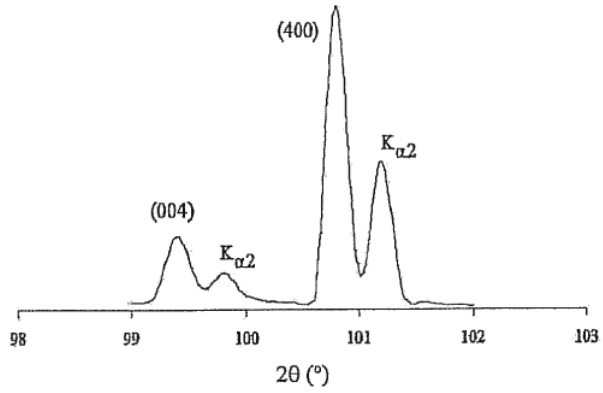

Fig. 10. Split peak in tetragonal barium titanate for BT sample (pure $BaTiO_3$) sintered at 1300°C for 2 h.

transfer function of the sensing elements can be expressed using a polynomial equation; then, it can be deduced that the BTLP samples are not suitable for high-relative-humidity applications. As the PMMA content increased, i.e., in the case of BTLP-3, the transfer functions indicated higher electrical conductivities. When the working temperature was increased to 80°C, a considerable increase in electrical conductivity was observed.

After sintering at 1300°C for 2–6 h, the humidity sensitivity curves were linear, indicating that the sensing elements were sensitive for all the relative humidities considered. The humidity sensitivities were higher for the samples sintered at 1200°C. However, when the BTLP compositions were sintered at 1500°C, the linearity characteristic degraded. On the other hand, a nonsensitive region, called the dead band, was observed for all the sintering times. Below a relative humidity of 40%, the BTLP samples were slightly sensitive or nonsensitive to humidity. This restricts the application of the sensing elements for lower relative humidities. Table 3 compares the humidity sensitivities of several sensing elements with those in the present study.

To sum up, the existence of a saturation limit (1300°C) and lack of linearity (slightly 1300 and 1500°C) below and above a certain relative humidity, also the dead band, made it difficult to use those sensing elements for sensor applications despite high conductivities.

There is a slight or no saturation limit for the compositions sintered at 1300°C, which made it beneficial for humidity sensing. The linearity characteristic, the highest correlation factor R^2 of which was determined to be 0.9978, is high. This value was obtained for BTLP-1 sintered at 1300°C for 6 h. The linear region of the transfer function shows the practical application range of the sensing element. Following a sintering process at 1500°C, the linearity characteristic of the transfer functions worsened further and a dead band region was observed. The sintering temperature was the main

Table 3
Comparison of several humidity-sensing elements.

Log ($R_{\%20}/R_{\%98}$)	Relative humidity (%)	Composition	Reference
454	5–98	$ZnCr_2O_4$-ZnO composite	Pokhrel *et al*.[4]
1000	10–98	$BaTiO_3$/polystyrene sulfonic sodium (PSS) film	Wang *et al*. [12]
100	30–90	Al_2O_3 substrate, sol-gel $BaTiO_3$ thin film	Yuk and Troczynski [13]
1000	30–100	$BaTiO_3$-polymer RMX composite	Wang *et al*.[14]
1000	30–90	Nanocrystalline $BaTiO_3$	Wang *et al*.[12]
120	11–94	Organic silicone polyelectrode (Si-PE)	Yao and Yang[15]
1000	10–95	Barium stanate ($Ba_{1-x}La_xSnO_3$)	Upadohyay and Kavitha[16]
1000	30–90	PMMA-(KOH/K_2CO_3) alkaline salts	Su *et al*.[17]
100	20–100	Barium titanate	Present study

parameter that determines the characteristic of the transfer functions, but the sintering time only affected the electrical conductivities in the range of 2–6 h.

Humidity hysteresis is one of the most important sensor characteristics and it must be as small as possible. The humidity hysteresis in the present study is between the literature hysteresis range for $BaTiO_3$-based ceramics, i.e., 6–8%RH. The humidity hysteresis was affected by the porosity. Thus, both for relative humidity increase and decrease, hysteresis occurred. The hysteresis values showed an area instead of a curve. The humidity adsorption and desorption processes are related to the attraction forces between water vapour and the surface. In the adsorption process, the oxygen atom is located in the oxygen vacancy, V_o^{++}, and induces the adsorption of hydroxide ions, OH^-. Naturally, a small number of oxygen vacancies are present in La_2O_3-doped barium titanate. That is why the adsorption rate is low in doped barium titanate. The desorption process includes the decomposition of adsorbed hydroxide ions and the formation of water vapour, leaving adsorbed oxygen on the surface and resulting in the breaking of the bonds. Thus, this process requires energy. That is why the response time for the desorption process is longer and the hysteresis occurs.[11]

For several sensing elements, the comparison of the hysteresis values is given in Table 4. The silicone, which is used in the electronic applications and different coatings, is given in the table. For nano- and organic silicone structures, the same type of 2-acrylamido-2-methylpropane sulfonic acid (AMPS) is used as the additive. The hysteresis values of barium strontium titanate (BST) and $BaTiO_3$-based thin films are minimum and that of organic silicone is relatively higher. The hysteresis values of nano-$BaTiO_3$ and silicone are similar. Copper titanate and barium strontium titanate coatings have comparable hysteresis values. The humidity hysteresis of PMMA is 3% in a range of 30–90% of relative humidity. The humidity hysteresis of the $BaTiO_3$-polymer composite is similar to that of PMMA.

Table 4
Comparison of hysteresis values for various sensing elements.

Hysteresis value (%)	Relative humidity (%)	Sensing element	Reference
5,9	30–90	Organic silicone sol/poly-AMPS	Su and Uen[18]
1,17	30–90	Nano-SiO_2 powder/poly-AMPS	Su and Uen[18]
2	20–95	TiO_2-Cu_2O-Na_2O copper titanate thick film	Kim and Gong[19]
2	10–98	BST thin film	Agarwal and Sharma[20]
1	30–90	Al_2O_3 substrate sol-gel $BaTiO_3$ thin film	Yuk and Troczynski[13]
3	33–98	$BaTiO_3$-polymer RMX composite	Wang *et al.*[14]
3	30–90	Nanocrystalline $BaTiO_3$	Wang *et al.*[12]
2	12–94	Organic silicone polyelectrode (Si-PE)	Yao and Yang[15]
4	30–90	PMMA-(KOH/K_2CO_3) alkaline salts	Su *et al.*[17]
5	10–98	Barium titanate	Present study

As shown in Fig. 9, first, the sample with BTLP-3 was subjected to a relative humidity of 30% and the conductivity ($\sigma(0)$) of $10^{-5.5}$ S·m^{-1} was detected when the humidity was increased to 98%; this conductivity indicated a sharp increase and a stable conductivity ($\sigma(\infty)$) of $10^{-3.5}$ S·m^{-1} was obtained. The duration required to reach the latter conductivity was considered the response time of 60 s. After reaching the stable conductivity at 98%, relative humidity was reduced to a lower value of 30% and the duration required to reach a constant conductivity at 30% was considered the recovery time of 120 s for the BTLP-3 composition. The desorption duration of the porous BTLP-3 composition was twice the absorption duration.

5. Conclusions

Porous barium titanate ceramics were fabricated by the addition of PMMA. PMMA addition resulted in a slight grain refinement. The grain size of BTLP-1 containing 1 wt% PMMA was measured to be 14.87 μm, whereas that of BTLP-3 containing 2.5 wt% PMMA was measured to be 13.75 μm after sintering at 1500°C for 6 h. For BTLP-3 the first endothermic reaction occurred at 832.7°C, which corresponds to the orthorhombic-hexagonal transformation of barium carbonate. The formation of barium titanate occurred at 1125°C for BTLP-3. Since the linearity, dead band region and saturation limit characteristics are the main parameters affecting the practical sensor applications, sintering temperatures were determined to be the main parameter for changing the availability of different compositions for several uses. For the compositions studied, the maximum humidity hysteresis was a relative humidity of 5%.

References

1 B. R. Eggins: Chemical Sensors and Biosensors (John Wiley and Sons, London, 2002) p. 20.
2 I. Sinclair: Sensors and Transducers (Newnes, London, 2001) p. 170.
3 V. Matko and D. Donlagic: Sens. Actuators, A **61** (1997) 331.
4 S. Pokhrel, B. Jeyaraj and K. S. Nagaraj: Mater. Lett. **57** (2003) 3543.
5 K. S. Chou, T. K. Lee and F. J. Liu: Sens. Actuators, B **56** (1999) 106.
6 C. R. M. Rao and P. N. Mehrotra: J. Therm. Anal. Calorim. **17** (2005) 539.
7 C. J. Peng and H.Y. Lu: Communications of the American Ceramic Society **71** (1988) 44.
8 J. Qi, L. Li, Y. Wang, Y. Fan and Z. Gui: Mater. Chem. Phys. **82** (2003) 423.
9 E. Brzozowski and M. S. Castro: J. Eur. Ceram. Soc. **24** (2004) 2499.
10 S. Chatterjee, B. D. Stojanovic and H. S. Maiti: Mater. Chem. Phys. **78** (2003) 702.
11 T. Islam and H. Saha: Sens. Actuators, B **114** (2006) 334.
12 J. Wang, B. K. Xu, G. F. Liu, J. C. Zhang and T. Zhang: Sens. Actuators, B **66** (2000) 159.
13 J. Yuk and T. Troczynski: Sens. Actuators, B **94** (2003) 290.
14 J. Wang, W. Yan, J. Zhang, F. Qiu, T. Zhang, G. Liu and B. Xu: Mater. Chem. Phys. **69** (2001) 288.
15 Z. Yao and M. Yang: Sens. Actuators, B **117** (2006) 93.
16 S. Upadhyay and P. Kavitha: Mater. Lett. **61** (2007) 1912.
17 P. G. Su, Y. L. Sun and C. C. Lin: Sens. Actuators, B **113** (2006) 883.
18 P. G. Su and C. L. Uen: Talanta **66** (2005) 1247.
19 D. Kim and M. S. Gong: Sens. Actuators, B **110** (2005) 321.
20 S. Agarwal and G. L. Sharma: Sens. Actuators, B **85** (2002) 205.